ISSN Online: 2756-3898, ISSN Print: 2714-500X https://doi.org/10.47514/phyaccess.2025.5.1.010

First-Principle Study of Optical Properties in Erbium-Doped Fibres for Enhanced Optical Signal Amplification

Umaru B Machu[1], Haruna Ali[1], Mohammed Y Onimisi[1], Joshua A Owolabi[1], Christiana O Akusu[1], Hassan G Muhammad[1], Ugbe R Ushiekpan[1], Abubakar Dalhat[1], Stephen C Nnochin[1], Alhassan Shuaibu[2] and Isaac H Daniel[2]

[1] Department of Physics, Nigerian Defence Academy, Kaduna State, Nigeria
[2] Department of Physics, Kaduna State University, Kaduna State, Nigeria

Corresponding E-mail: machubenedict@gmail.com

Received 26-03-2025
Accepted for publication 29-04-2025
Published 02-05-2025

Abstract

The optical properties of silica, essential for applications ranging from fibre optics to UV transmission windows, are closely linked to atomic-scale defects, even though they are challenging to identify. Although electron paramagnetic resonance (EPR) has long been the predominant technique for defect analysis, this study employs time-dependent density functional perturbation theory (TDDFPT) to systematically examine the understudied optical signatures of erbium (Er)-doped silica (SiO_2) and native defects (oxygen/silicon vacancies). The Er-doped systems (2.08–6.25% concentrations) and pure SiO_2 along vacancy defects were simulated to compute transmittance, reflectivity, dielectric characteristics, and absorption. The results showed that the absorption peaks and imaginary dielectric function (ε_2) are redshifted by Er inclusion, with doping at 4.17% yielding the best improvement. Conversely, vacancy defects decrease otherwise because of increased absorption and reflection of the visible spectrum. These findings demonstrate how Er-doping can alter SiO_2's optical response and emphasize the value of TDDFPT in connecting optical behaviour to defect patterns. This study advances the logical design of silica-based optoelectronic devices and offers a theoretical foundation for enhancing defect engineering in wide-gap semiconductors.

Keywords: Silica; Erbium doping; Optical properties; TDDFPT; Defect engineering; Dielectric function.

I. INTRODUCTION

The optical properties of silica are often one of the most important aspects of glassy applications [1]. They are reasonably easy to measure with standard spectrophotometers and offer instantaneous information on the quality of important silica-based devices, such as the attenuation of ultraviolet (UV) transmission windows [2] or fibre-optic waveguides [3]. However, optical measurements alone are usually sufficient to determine the origin and atomic structure of the related point defects. The bulk of the information on the structures of defects in silica over the past few decades has come from electron paramagnetic resonance (EPR) studies since they are the most effective at "seeing" the atomic environment of the unpaired electron of a paramagnetic defect [4].

Due to EPR, optical spectroscopy has largely been overlooked in fundamental defect research. It was once thought that identifying a colour centre in silica involved two

steps: (i) figuring out the atomic structure of the defect using EPR, and (ii) figuring out which optical band, if any, coincides with the EPR signal. Only a small number of defect centres have demonstrated reliable correlations between the optical and EPR signals, and the second part of this study has proven to be quite difficult. Optical spectroscopy is particularly useful when EPR techniques are not appropriate, such as for diamagnetic defects, or when EPR optical correlations are distorted by inhomogeneous broadening effects [5].

Time-dependent density functional perturbation theory (TDDFPT) has recently been recognized as one of the most effective methods for accurately predicting optical properties within all defect centres [6]. As a result, many researchers have used TDDFPT to study how defects affect the optical properties of various wide-gap semiconductors [7], [8], yielding several results close to the experimental values for many applications. Lately, the focus of research has been on defects caused by Rare-earth (RE) doping in wide-gap semiconductors like silica, ZnO, etc. Reference [9] investigated the effects of an Er-defect on the optical characteristics of zinc oxide (ZnO) and discovered that Er-doped ZnO is an excellent dielectric material for high-frequency device applications. To our knowledge, a systematic investigation into the optical properties of defect states in silica has not yet been reported. In this study, we examine the effects of erbium-related defects on the optical behaviour of silica to advance the understanding of defect-induced optical modifications in this material.

II. MODEL AND METHOD

A. Model

As the primary material, we systematically modelled pure silica (SiO_2), which has a tetragonal structure and is a member of the P42/mbc (135) space group. Its symmetry is 4/mmm. In the unit cell, the structure is made up of 16 Si and 32 O atoms. The doping modelling was done by substituting one Si atom with one Er, which is equivalent to 2.08%, two Si atoms with two Er, which is equivalent to 4.17%, and finally three Si atoms with three Er atoms, which is equivalent to 6.25% doping concentration. The effect of interstitial defects was further examined by removing one O atom from the optimized pure SiO_2, which is known as an oxygen vacancy defect (O_v), and then removing another Si atom, which is known as a silicon vacancy defect (Si_v).

B. Computational Method

The optical characteristics of optoelectronic devices, such as light sources and detectors, are crucial to their designs and analyses. These characteristics are represented by the optical dielectric function. At all photon energies, the combined density of states and optical matrix elements are highly correlated with the imaginary component $i\varepsilon_2(\omega)$ of the complex dielectric function by (1).

$$\varepsilon(\omega) = \varepsilon_1(\omega) + i\varepsilon_2(\omega) \quad (1)$$

Where ω is the frequency, $\varepsilon_1(\omega)$ is the real part, governing dispersion, and $\varepsilon_2(\omega)$ is the imaginary part, related to absorption and loss. The actual portion $\varepsilon_1(\omega)$ is obtained from $i\varepsilon_2(\omega)$. Both interband and intraband transitions affect $\varepsilon(\omega)$. In this study, the indirect interband transitions, which entail phonon scattering and are assumed to contribute marginally to $\varepsilon(\omega)$ were neglected.

III. RESULTS AND DISCUSSION

A. Optical Absorption Coefficient

In Fig. 1(a), Er-doped SiO_2 shows the black curve for pure SiO_2, which provides the baseline of these results. A first major absorption peak at ≈ 12.5 eV with an absorption coefficient of about 2.5×10^4 cm^{-1} arises from O 2p nonbonding electrons excited into the Si 3p antibonding conduction band just above the fundamental gap (the 8.0 – 9.0 eV optical gap), and a second, stronger resonance at ≈ 16.5 eV (≈ 3.0×10^4 cm^{-1}) originates from deeper O 2p bonding levels with excitonic enhancement into higher-lying Si 3d/4s conduction states [10], [11].

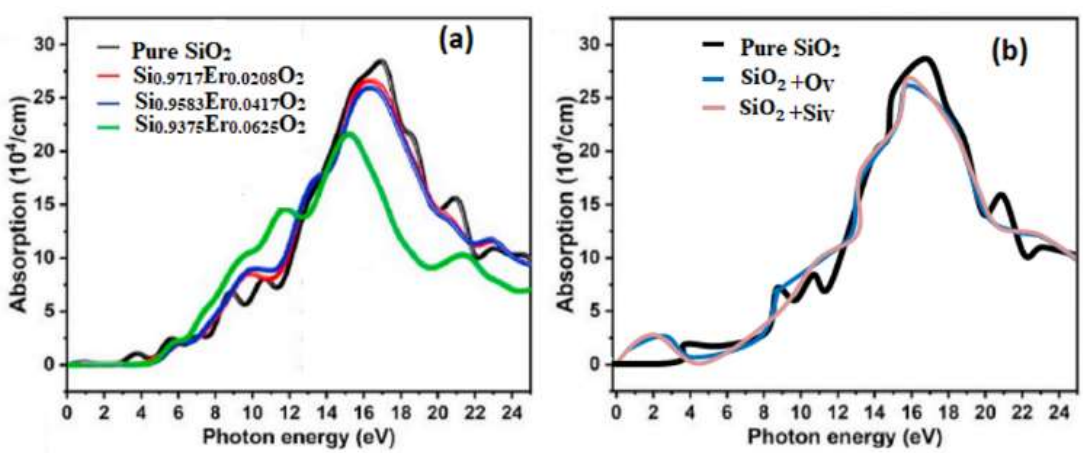

Fig. 1. Calculated optical absorption coefficient of (a) pure SiO_2, $Si_{0.9717}Er_{0.0283}O_2$, $Si_{0.9583}Er_{0.0417}O_2$ and $Si_{0.9375}Er_{0.0625}O_2$ (b) pure SiO_2, SiO_2 + O_v and SiO_2+Si_v

Introducing Er^{3+} systematically perturbs these features; the red curve (x = 0.0208) exhibits its main UV peak shifted down to ≈ 12.3 eV and reduced to ≈ 2.4 × 10^4 cm^{-1}, indicating heavy Er^{3+} ions perturb the local Si–O network and mix Er 5d character into the conduction band [12]. Increasing the Er-doping concentration to x = 0.0417 (blue curve) pushes that peak to ≈ 12.2 eV at 2.3 × 10^4 cm^{-1}, while the secondary UV resonance near 16 eV likewise shifts and broadens [13]. At the highest Er concentration (x = 0.0625, green curve), the primary UV peak shifts to ≈ 12.0 eV with an intensity of only ≈ 2.0 × 10^4 cm^{-1}, reflecting maximal lattice distortion and enhanced Er 4f–5d conduction-band hybridization that together lower the effective band-edge energy and diminish oscillator strength, thus producing a pronounced red shift and peak attenuation [14]. Across all doped curves, the gradual red shift and peak-height reduction illustrate how increasing Er concentration introduces intra-atomic 4f–5d transitions in the gap region (visible as faint shoulders near 3.0 – 5.0 eV) and perturbs the host's UV interband resonances [15], [16].

Fig. 1(b) compares pure SiO_2 (black) with two intrinsic defect scenarios. In the defect-engineered samples, both the oxygen-vacancy curve (blue) and the silicon-interstitial curve (brown) retain the two principal UV peaks near 12.0 –17.0 eV but each is slightly broadened and red-shifted by ≈ 0.1 eV due to the disrupted Si–O network relative to pure SiO_2; additionally, new sub-band-gap shoulders appear at 3.0 – 5.0 eV, marking optical transitions from defect-localized gap states into the conduction band, which give rise to visible-range absorption absent in pristine silica [17, [18]. For silicon interstitials (brown curve), mid-gap states produce a subgap absorption feature around 3.0 – 5.0 eV, while the UV peaks at ≈ 12.3 eV (≈ 2.3 × 10^4 cm^{-2}) and ≈ 16.4 eV (≈ 2.7 × 10^4 cm^{-1}) are again slightly red-shifted and broadened relative to pure SiO_2 [19]. Together, these defect curves show that network disruptions, whether by missing oxygen or extra silicon create localized electronic levels inside the fundamental gap that absorb visible photons and simultaneously perturb the high-energy interband and excitonic resonances inherited from the O 2p → Si 3p/3d transitions of the undisturbed matrix. The calculated optical absorption coefficient peak characteristics variations are shown in Table I.

Table I. Calculated optical absorption coefficient peak characteristics variations.

Material	Peak Energy (eV)	Peak Intensity (10^4 cm^{-1})	Peak Shape	Likely Cause
Pure SiO_2	13.0 – 14.0	25.0 – 27.0	Broad	Interband transitions.
$Si_{0.9717}Er_{0.0208}O_2$	13.0	22.0 – 24.0	Broad	induced additional states.
$Si_{0.9583}Er_{0.0417}O_2$	13.0 – 14.0	27.0 – 28.0	Broad, intense	Higher Er doping enhances absorption.
$SiO_2 + O_v$	13.0	27.0 – 28.0	Sharp, intense	O_v states near the conduction band.
$SiO_2 + Si_v$	13.0 – 14.0	25.0 – 26.0	Broad, shoulder	Si_v states near the valence band.

B. Optical Transmittance Coefficient

Fig. 2(a) illustrates the optical transmittance of pure SiO_2 and SiO_2 doped with erbium (Er) at concentrations of 4.17% ($Si_{0.9583}Er_{0.0417}O_2$), 6.25% ($Si_{0.9375}Er_{0.0625}O_2$), and 12.5% ($Si_{0.9717}Er_{0.0208}O_2$). The pure SiO_2 (black curve) exhibits a peak transmittance of ~85% at ~3.0 eV (~413 nm) and falls below 20% by 12.0 eV (~103 nm), reflecting its intrinsic band-edge absorption [20]. At 12.5% Er, the peak transmittance decreases to 60% at 3.0 eV with a pronounced red shift, and transmittance plunges below 5% at 12.0 eV due to additional Er^3-related absorption centres [21]. In the 2.08% Er sample (red curve), transmittance remains high in the visible (1.65 – 3.1 eV), peaking at 85% at 3 eV, then decreases sharply, falling below 20% at 12.0 eV and approaching 0% at 20.0 eV; this behaviour is typical of low-concentration Er^{3+}-doped silica produced via sol–gel processes [22], and is governed by Er 4f–4f and charge-transfer transitions [23]. At 4.17% Er (blue curve), the visible-range peak is ~75% at 3.0 eV with UV transparency enhanced: transmittance rises to ~30% between 12.0 – 14.0 eV compared to near-zero in undoped SiO_2, suggesting that moderate Er doping passivates native defects (e.g. non-bridging oxygen-hole centres and E′ centres), reducing UV absorption [24], [25] With 6.25% Er (green curve), peak transmittance falls to 70% at 3.0 eV and declines to 10% by 12.0 eV, indicating that higher Er concentrations introduce a greater density of localized electronic states within the bandgap that enhance visible-range absorption [26]. The trend of decreasing peak transmittance (85% → 75% → 70% → 60%) and red shifting with increased Er content is consistent with the progressive introduction of electronic defect states by Er^{3+} ions [27].

Fig. 2(b) compares pure SiO_2 with oxygen-vacancy ($SiO_2 + O_v$, yellow curve) and silicon-vacancy ($SiO_2 + Si_v$, cyan curve) samples. Oxygen vacancies reduce the peak transmittance to ~60 % at 3.0 eV and produce a rapid drop to 10% by 10.0 eV, approaching 0% by 18.0 eV, showing that O_v acts as strong absorption/scattering centres [28]. Silicon vacancies have an even stronger effect, lowering the peak to ~50% at 3.0 eV and causing transmittance to fall below 5% by 10.0 eV, due to deep-level traps and significant lattice disruption [29], [30]. Both O_V and Si_v substantially diminish SiO_2's transmission, with Si_v having the more pronounced

impact (50% vs 60% peak transmittance). The steeper declines and spectral fluctuations between 6.0 – 12.0 eV indicate the creation of midgap states that increase absorption across the UV–Vis range [31]. The Optical Transmittance Peaks with key observations are depicted in Table II.

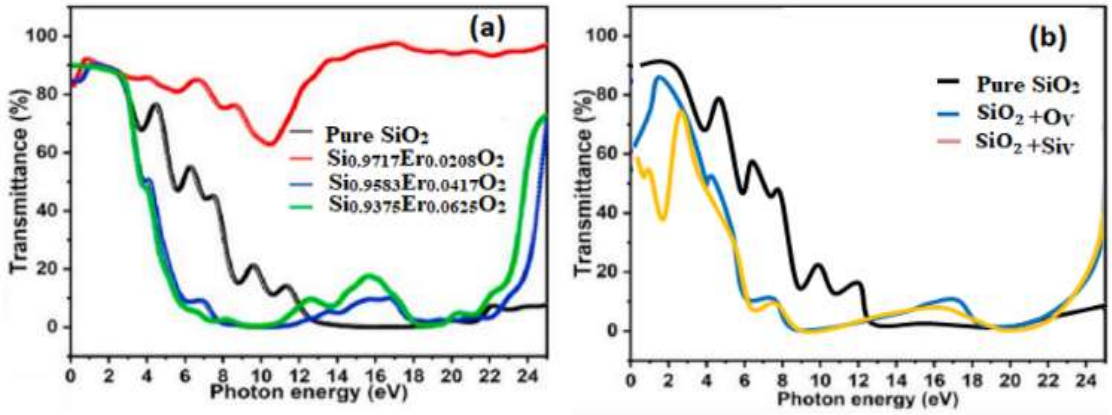

Fig. 2. Transmittance Coefficient of (a) pure SiO_2, $Si_{0.9717}Er_{0.0283}O_2$, $Si_{0.9583}Er_{0.0417}O_2$ and $Si_{0.9375}Er_{0.0625}O_2$ (b) pure SiO_2, SiO_2 + O_v and SiO_2+ Si_v

Table II. Optical Transmittance Peaks.

Sample	Colour in Fig. 2	Peak Transmittance (%T)	Photon Energy at Peak (eV)	Region	Key Observation
Pure SiO_2 (a)	Red	85.0	3.0	Visible	High transparency in the visible range.
$Si_{0.9583}Er_{0.0417}O_2$	Blue	75.0 (30.0 in UV)	3.0 (12 – 14 in UV)	Visible, UV	Increased UV transmittance at 4.17% Er.
$Si_{0.9375}Er_{0.0625}O_2$	Green	70.0	3.0	Visible	Decreased transmittance, slight red shift.
$Si_{0.875}Er_{0.125}O_2$	Black	60.0	3.0	Visible	Further decrease, pronounced red shift.
Pure SiO_2 (b)	Black	85.0	3.0	Visible	Baseline high transmittance.
SiO_2 + O_v	Yellow	60.0	3.0	Visible	Reduced transmittance due to O_v.
SiO_2 + Si_v	Cyan	50.0	3.0	Visible	Strongest reduction due to Si_v.

C. Dielectric function

Fig. 3 presents the imaginary part of the dielectric function (ε_2) for various silica-based materials, offering a window into their dielectric and optical properties across the energy range of 0 to 24.0 eV [32]. The dielectric function, a complex quantity expressed in (1), describes how the material interacts with electromagnetic radiation [33]. The imaginary part, ε_2, specifically relates to energy dissipation and absorption [34], while the real part, ε_1, is associated with polarization and refraction [35]. Since Fig. 3 focuses on ε_2, the dielectric properties were delved into, exploring the implications of the observed peaks, such as the effects of erbium doping and non-stoichiometric modifications, and their broader significance for optical and electronic applications. This analysis also ties these observations to the relationships between ε_2 and other optical parameters, such as the extinction coefficient, absorption coefficient, and reflectivity [36]. The dielectric function quantifies a material's response to an electric field, such as incident light. The imaginary part, ε_2, is directly proportional to the material's ability to absorb energy from the electromagnetic wave, reflecting processes like interband transitions, excitonic effects, or defect-related absorption [37]. Peaks in ε_2 indicate energies where these absorption processes are most pronounced and manifest as critical points in the joint density of states [38].

Fig. 3(a) compares pure SiO_2 (black), $Si_{0.9717}Er_{0.0208}O_2$ (red), $Si_{0.9583}Er_{0.0417}O_2$ (blue), and $Si_{0.9375}Er_{0.0625}O_2$ (green), showing the effect of increasing erbium doping. Fig. 3(b) compares pure SiO_2 (black), SiO_2 + O_v (blue), and SiO_2 + Si_v (yellow), illustrating the impact of oxygen and silicon excess. The

energy range of 0 – 24.0 eV corresponds to the ultraviolet (UV) and vacuum-UV spectrum, where silica-based materials typically exhibit strong absorption due to their wide bandgap (~9.0 eV) [39] and multiple interband transitions [40]. The dielectric properties inferred from ε_2 are critical for applications such as optical coatings, waveguides, dielectric layers in electronics, and UV optics, where controlling absorption, refraction, and energy dissipation is essential [41]. Fig. 3(a) shows how erbium doping alters the dielectric properties of silica, as evidenced by changes in the magnitude and shape of ε_2 peaks. The pure SiO_2 (black curve) exhibits a primary peak at 10.0 – 12.0 eV (~10.4 eV, 11.6 eV) corresponding to the fundamental interband transitions near the bandgap edge, with an intensity of ~1.0 – 1.2 [42]. A secondary peak at 18.0 – 20.0 eV (e.g., 16.2 eV, 20.1 eV) arises from higher-energy core-electron resonances and plasmonic features [43]. In dielectric terms, these features indicate additional energy-dissipation channels at higher photon energies, though less dominant than the bandgap absorption. Er-doping (red, blue, green curves) systematically increases the intensity of both the primary (to ~1.5 – 3.0) and secondary (to ~0.8–1.5) ε_2 peaks, reflecting the introduction of erbium-related electronic states that enhance absorption and dielectric loss in the UV [44]. $Si_{0.9717}Er_{0.0208}O_2$ shows moderate enhancement (primary ~1.5 – 1.8; secondary ~ 0.8–1.0), $Si_{0.9583}Er_{0.0417}O_2$ stronger (primary ~ 2.0 – 2.5; secondary ~1.0 – 1.2), and $Si_{0.9375}Er_{0.0625}O_2$ the most pronounced (primary ~2.5 – 3.0; secondary ~1.2 – 1.5). This trend implies an increasing density of erbium-related defect or impurity states that facilitate UV absorption, which can be exploited in applications like UV filters, sensors, or photonic devices requiring controlled absorption [45].

Fig. 3(b) illustrates that oxygen vacancies ($SiO_2 + O_v$) introduce sub-bandgap absorption features (e.g., around 7.6 eV) due to defect-level transitions [46], while silicon excess ($SiO_2 + Si_v$) similarly modifies the UV absorption profile through Si-related dangling-bond states. These defect-induced absorption bands broaden ε_2 and increase dielectric loss, impacting the transparency and performance of SiO_2 dielectrics in UV-critical applications [47]. The dielectric properties based on ε_2 peaks are presented in Table III.

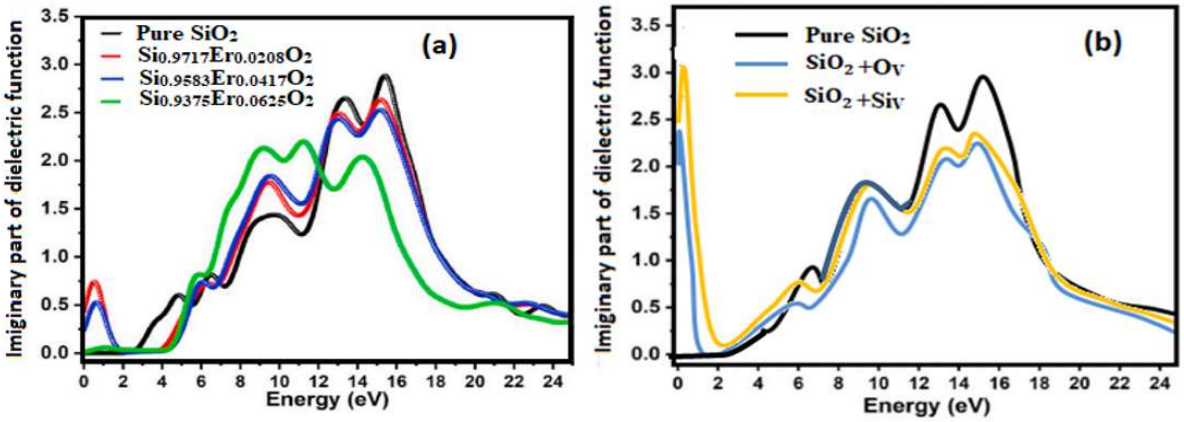

Fig. 3. The imaginary part of the dielectric function of (a) pure SiO_2, $Si_{0.9717}Er_{0.0283}O_2$, and $Si_{0.9583}Er_{0.0417}O_2$, and $Si_{0.9375}Er_{0.0625}O_2$ (b) $SiO_2 + O_v$ and $SiO_2 + Si_v$

Table III. Dielectric Properties Based on ε_2 Peaks.

Material	Colour in Fig. 3	Primary Peak (eV)	Primary Peak Intensity	Secondary Peak (eV)	Secondary Peak Intensity	Dielectric Loss Implication
Pure SiO_2	Black	10.0-12.0	1.0-1.2	18.0-20.0	0.5-0.7	Low loss, suitable for low-loss dielectrics.
$Si_{0.9717}Er_{0.0283}O_2$	Red	10.0-12.0	1.5-1.8	18.0-20.0	0.8-1.0	Moderate loss, increased absorption.
$Si_{0.9583}Er_{0.0417}O_2$	Green	10.0-12.0	2.0-2.5	18.0-20.0	1.0-1.2	Higher loss, stronger absorption.
$Si_{0.9375}Er_{0.0625}O_2$	Blue	10.0-12.0	2.5-3.0	18.0-20.0	1.2-1.5	Highest loss in Fig. 3(a), strongest absorption.
$SiO_2 + O_v$	Blue	8.0-10.0	2.0-2.5	18.0-20.0	0.8-1.0	High loss, shifted absorption due to defects.
$SiO_2 + Si_v$	Yellow	8.0-10.0	2.5-3.0	18.0-20.0	1.0-1.2	Highest loss in Fig.3(b), strongest absorption.

D. Reflectivity coefficient

Fig. 4(a) presents the reflectivity of pure SiO_2 and Er-doped SiO_2 as a function of photon energy, with each sample represented by a distinct colour to facilitate comparison [48]. The reflectivity curves reveal how erbium doping modifies the optical properties of SiO_2, particularly in the UV range [49]. The Pure SiO_2 (Black Curve) shows a gradual increase in reflectivity with increasing photon energy. It reaches a peak reflectivity of approximately 0.15 (15%) around 20.0 – 22.0 eV, indicating that 15% of the incident light is reflected at these high energies in the UV region. This relatively low reflectivity underscores SiO_2's transparency in the visible range and moderate reflectivity in the UV range, consistent with its use in optical applications [50]. In the $Si_{0.9717}Er_{0.0208}O_2$ (2.0% Er, Red Curve), the reflectivity increases more rapidly than in pure SiO_2, peaking at approximately 0.20 (20 %) around 18.0 – 20.0 eV [51]. This enhancement suggests that even a small amount of Er doping introduces electronic states that increase light reflection, particularly in the UV region [52]. The slight shift in peak energy compared to pure SiO_2 indicates a modification in the material's band structure. For the $Si_{0.9583}Er_{0.0417}O_2$ (4.1% Er, Blue Curve), at a higher Er concentration of 4.1%, the peak reflectivity rises to 0.22 (22%) at 18 eV. The peak is sharper and more pronounced than in the 2.0% Er sample, reflecting a stronger influence of erbium on the material's optical properties. This increase in reflectivity suggests that additional Er ions create more defect-related energy levels, enhancing light scattering or reflection [53]. Finally, in the $Si_{0.9375}Er_{0.0625}O_2$ (6.2% Er, Green Curve), the reflectivity reaches its maximum at 0.25 (25%) at 18.0 eV, the highest among all samples. This peak is not only higher but also occurs at well-defined energy, indicating that higher Er doping significantly alters the electronic structure of SiO_2, leading to increased reflectivity in the UV range. The Reflectivity Coefficient Peaks of the samples are shown in Table IV.

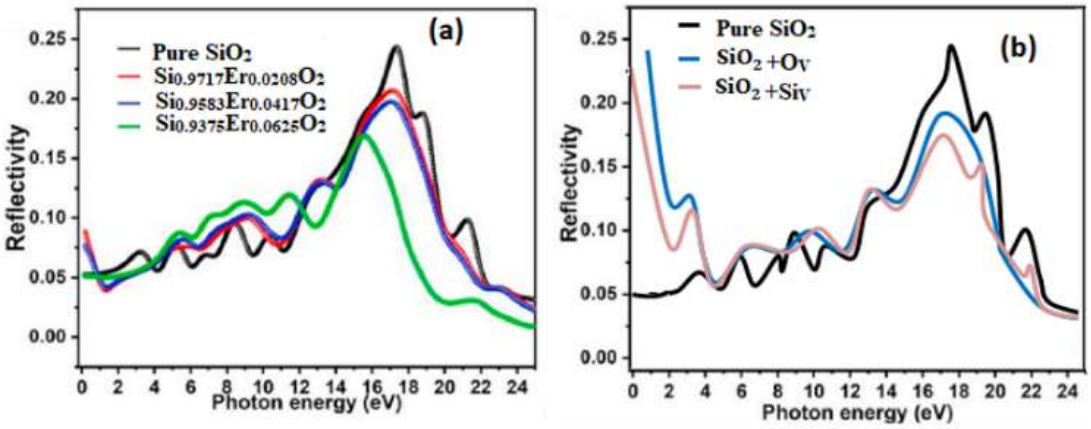

Fig. 4. Reflectivity coefficient of (a) pure SiO_2, $Si_{0.9717}Er_{0.0283}O_2$, $Si_{0.9583}Er_{0.0417}O_2$ and $Si_{0.9375}Er_{0.0625}O_2$ (b) pure SiO_2, SiO_2 + O_v and SiO_2+ Si_v.

Table IV. Reflection Coefficient Peaks.

Sample	Colour in Fig. 4	Peak Reflectivity	Photon Energy at Peak (eV)	Region
Pure SiO_2 (a, b)	Black	0.15	20.0–22.0	UV
$Si_{0.971}Er_{0.0208}SiO_2$ (2.0% Er)	Red	0.20	18.0–20.0	UV
$Si_{0.953}Er_{0.041}SiO_2$ (4.1% Er)	Green	0.22	18.0	UV
$Si_{0.937}Er_{0.062}SiO_2$ (6.2% Er)	Blue	0.25	18.0	UV
SiO_2 + O_v	Blue	0.20	18.0	UV
SiO_2 + Si_v	Pink	0.22	18.0	UV

Fig. 4(b) shows the impact of native defects, oxygen vacancies (O_v) and silicon vacancies (Si_v), on the reflectivity of SiO_2 [53]. These defects introduce structural and electronic changes that alter the material's optical properties, with each sample represented by a distinct colour. The Pure SiO_2 (Black Curve), consistent with Fig. 4 (a), serves as the reference, peaking at 0.15 (15%) around 20.0 – 22.0 eV. This baseline reflectivity reflects the intrinsic optical properties of SiO_2, with moderate reflection in the UV range and high transparency in the visible spectrum [54]. The SiO_2 + O_v (Blue Curve) shows that the introduction of oxygen vacancies increases the reflectivity, with a peak of approximately 0.20 (20%) at 18.0 eV. This enhancement indicates that O_v creates defect states within the band gap that increase light scattering or reflection, particularly in the UV range [55]. The peak at 18.0 eV suggests a shift in the optical response compared to

pure SiO_2, similar to the effect observed with Er doping. In contrast, the $SiO_2 + Si_v$ (Pink Curve) shows that silicon vacancies have a more significant impact, with a peak reflectivity of 0.22 (22%) at 18.0 eV [56]. The curve for $SiO_2 + Si_v$ is sharper than that for $SiO_2 + O_v$, indicating a more localized effect on the material's optical properties [57]. The rapid decline after the peak suggests that Si_v introduces deep donor levels that enhance reflectivity within a narrow energy range, particularly in the UV region.

IV. Conclusion

The combined optical and dielectric analyses show that both erbium doping and intrinsic defect offer strong ways to customise the UV–visible response of silica. The incorporation of Er^{3+} attenuates and redshifts the primary interband absorption peaks (from ≈12.5 eV to ≈12.0 eV) while introducing weaker intra-4f–5d resonances in the 3 – 5 eV range. In turn, transmittance in the visible decreases (85% to 60% at 3 eV) as Er concentration increases, while dielectric loss (ε_2) and reflectivity in the UV both rises, reflecting improved absorption channels and altered band-edge structure. The Si–O network is similarly perturbed by silicon interstitials and oxygen vacancies: each defect species produces sub-bandgap shoulders around 3 – 5 eV, increases dielectric loss and reflectivity at 18 eV, and redshifts and broadens the ≈12 – 17 eV UV resonances by ∼0.1 eV. The unique electronic fingerprints of various defect types are highlighted by the significantly higher midgap absorption and reflectivity enhancement exerted by silicon interstitials compared to oxygen vacancies. These findings, together measure the extent to which silica's optical edge, absorption strength, and dielectric behaviour may be engineered using rare-earth doping and regulated defect populations. Such tunability benefits the design of UV-optical coatings, photonic devices, and dielectric layers, where precise control of band-edge absorption, transmittance, and energy dissipation is essential.

References

[1] K. Aly. "Adjusting the relation between the imaginary part of the dielectric constant and the wavelength". *Physica B: Cond. Matt., vol. 655*, pp. 414723, 2023.

[2] T. H. Wu, et al. "Visible-to-ultraviolet frequency comb generation in lithium niobate nanophotonic waveguides". *Nat. Photonics*, vol. *18, no.* 3, pp. 218-223, 2024.

[3] H. T. Zubair, et al. "Recent advances in silica glass optical fibre for dosimetry applications". *IEEE Photonics J.*, vol. *12, no.* 3, pp. 1-25, 2020.

[4] G. Murtaza, N. Yousaf, M. Yaseen, A. Laref and S. Azam. "Systematic studies of the structural and optoelectronic characteristics of $CaZn_2X_2$ (X= N, P, As, Sb, Bi)". *Mat. Res. Exp.*, vol. *5*, no. 1, pp. 016304, 2018.

[5] J. Heller. "*Structure formation as studied by EPR spectroscopy: From simple solutions to nanoparticles".* PhD dissertation, Dept. of Chem., Pharm. & Geosci., Joh. Gut. Univ., Mainz, Ger., 2010.

[6] M. E. Casida and M. Huix-Rotllant. "Progress in time-dependent density-functional theory". *Annual Rev. of Phy. Chem.*, vol. *63*, no. 1, pp. 287-323, 2012.

[7] J. Cajzl, P. Nekvindová, A. Macková, M. Varga and A. Kromka. "Erbium ion implantation into $LiNbO_3$, Al_2O_3, ZnO and diamond–measurement and modelling – an overview". *Phy. Chem. Chem. Phy.*, vol. *24, no.* 32, pp. 19052-19072, 2022.

[8] G. Ohad, G., et al. "Optical absorption spectra of metal oxides from time-dependent density functional theory and many-body perturbation theory based on optimally-tuned hybrid functionals". *Phys. Rev. Mat.*, vol. *7, no.* 12, pp.123803, 2023.

[9] W. Y. Cong, Y. B. Lu, P. Zhang and C. B. Guan. "First principle study of electronic structures and optical properties of Ce-doped SiO_2". *AIP Adv.*, vol. *8, no.* 5, 2018.

[10] P. M. Schneider and W. B. Fowler. "Peaks in observed x-ray emission and optical-absorption spectra identified with critical points in the densities of states". *Phys. Rev. Lett.,* vol. 36, no. 425, 1976. DOI: 10.1103/PhysRevLett.36.425.

[11] S. S. Nekrashevich and V. A. Gritsenko. "Electronic structure of silicon dioxide (a review)". *Phys. Solid State, vol.* 56, no. 2, pp. 209–223, 2014. DOI: 10.1134/S106378341402022X.

[12] A. Abdullah, E. M. Benchafia, D. Cho and S. Abedrabbo. "Synthesis and Characterization of Erbium-Doped Silica Films Obtained by an Acid–Base-Catalyzed Sol-Gel Process. *Nanomat.*, vol. *13, no.* 9, pp. 1-13, 2023. https://doi.org/10.3390/nano13091508.

[13] I. H. El Azab, A. Ibrahim, M. Abdel El-Moneim, M. S. Zoromba, M. H. Abdel-Aziz, M. Bassyouni and A. F. Al-Hossainy. "A combined experimental and TDDFT-DFT investigation of structural and optical properties of novel pyrazole-1, 2, 3-triazole hybrids as optoelectronic devices". *Phase Trans.*, vol. *94, no.* 11, pp. 794-814, 2021.

[14] X. Guan, et al. "Electronic and optical properties of Ge-doped silica optical fibre". *Modern Phy. Lett. B*, vol. *33, no.* 12, pp. 1950150, 2019.

[15] N. Ullah, G. Murtaza, R. Khenata, J. Rehman, H. U. Din and S. B. Omran. "Structural, chemical bonding and optoelectronic properties of Mg-doped zinc chalcogenides: A first-principles study". *Mat. Sci. in Semicond. Proc.*, vol. *26*, pp. 681-689, 2014.

[16] R. Kitamura, L. Pilon and M. Jonasz. "Optical constants of silica glass from extreme ultraviolet to

far infrared at near room temperature". *App. Opt.*, vol. *46, no.* 33, pp. 8118-8133, 2007.

[17] S. Girard, A. Alessi, N. Richard, L. Martin-Samos, V. De Michele, L. Giacomazzi, S. Agnello, D. D. Francesca, A. Morana, B. Winkler, I. Reghioua, P. Paillet, M. Cannas, T. Robin, A. Boukenter and Y. Ouerdane. "Overview of radiation-induced point defects in silica-based optical fibres". *Rev. in Phy.*, vol. *4*, pp. 100032, 2019. https://doi.org/10.1016/j.revip.2019.100032.

[18] T. E. Tsai, J. M. Jewell and J. S. Sanghera. "Dynamics of the 5 eV optical absorption in SiO_2 glass". *J. App. Phy., vol.* 73, pp. 1501–1506, 1993. DOI: 10.1063/1.109028

[19] A. Marini, C. Hogan, M. Grüning and D. Varsano. "Yambo: an ab initio tool for excited state calculations". *Comp. Phy. Comm.*, vol. *180, no.* 8, pp. 1392-1403, 2009.

[20] A. Roy, et al. "Visible-to-mid-IR tunable frequency comb in nanophotonics. *Nat. Comm.*, vol. *14, no.* 1, pp. 6549, 2023.

[21] Y. Xu et al., "Enhanced photoluminescence of Er^{3+} in Si-rich SiO_2 films with optimized silicon content," Nanoscale Res. Lett., vol. 9, p. 456, 2014. doi: 10.1186/1556-276X-9-456.

[22] H. M. Mansour, M. G. El Sherbiny, A. M. ElKorashy, Y. S. El Sayed, H. I. El-Mously, and A. M. Abo El Ata, "Synthesis and optical properties of erbium-doped sodium silicate in sol-gel matrix," Silicon, vol. 16, pp. 3719–3727, 2024. doi: 10.1007/s12633-024-02947-4.

[23] J. R. Chelikowsky and M. Schlüter. "Electronic and optical properties of all polymorphic forms of silicon dioxide*". Phys. Rev. B, vol.* 15, pp. 4020–4032, 1977. DOI: 10.1103/PhysRevB.15.4020.

[24] E. Calabrese. "Electronic and optical properties of all polymorphic forms of silicon dioxide". *Phys. Rev. B, vol.* 18, pp. 2888–2896, 1978. DOI: 10.1103/PhysRevB.18.2888.

[25] J. H. Stathis. "Optically induced metastable defect states in amorphous silicon dioxide". Ph.D. dissertation, Dept. of Phy., MIT, Cambridge, MA, pp. 342, 1985.

[26] A. B. Smith. "Optical absorption in fused silica at elevated temperatures during 1.5-MeV electron irradiation." NASA Tech. Note D-6595, 1972.

[27] F. Gourbilleau, R. Rizk, C. Dufour, R. Madelon. "Fabrication and optical properties of Er-doped multilayers Si-rich SiO_2/SiO_2: size control, optimum Er–Si coupling, and interaction distance monitoring." Opt. Mat., vol. 27, no. 5, pp. 868–873, 2005.

[28] Th. Förster. "Intermolecular energy migration and fluorescence". Annalen der Physik, vol. 437, pp. 55-75, 1948. http://dx.doi.org/10.1002/andp.19484370105.

[29] D. L. Griscom. "Point Defects in Amorphous SiO_2: What Have We Learned from 30 Years of Experimentation?" MRS Proceed., vol. 61, pp. 213–221, 1985.

[30] A. Polman, et al. "Exciton–erbium interactions in Si nanocrystal-doped SiO_2." J. of App. Phy., vol. 76, no. 1, pp. 7–9, 2000.

[31] R. Salh, "Defect related luminescence in silicon dioxide network: A review". *Cryst. Si: Prop. & Uses*, S. Basu, Ed. Rijeka, Croatia: InTech., pp. 135–172, 2011.

[32] M. Oto, S. Kikugawa, N. Sarukura, M. Hirano, H. Hosono. "Optical fibre for deep ultraviolet light." IEEE Photonics Tech. Lett., vol. 13, no. 9, pp. 978–980, 2001.

[33] F. Liu, et al. "Effects of Radiation on Optical Fibers." Recent Prog. in Opt. Fiber Res. Intech, pp. 432–450, 2012.

[34] Dielectric Function Overview *Dielectric Function* – "an overview" *ScienceDirect Topics.* ScienceDirect. https://www.sciencedirect.com/topics/engineering/dielectric-function.

[35] Kramers-Kronig Consistency *Kramers–Kronig relations.* Wikipedia. https://en.wikipedia.org/wiki/Kramers–Kronig_relations

[36] M. Born and E. Wolf. "ε_2 and Optical Absorption". Principles of Optics, 7th ed., Cambridge University Press, 1999, pp. 114–116, 1999.

[37] J. A. Woollam. "Light and Materials". In Ellipsometry Tutorials. J. A. Woollam Co., Inc. https://www.jawoollam.com/resources/ellipsometry-tutorial/light-and-materials

[38] Critical Points in ε_2, N. W. Ashcroft and N. D. Mermin, "Solid State Physics," Holt, Rinehart and Winston, 1976, Sec. 26.2. MIT.

[39] SiO_2 Bandgap ≈ 9 eV, "List of band gaps" table, *Electromagnetic Spectrum* – Wikipedia. https://en.wikipedia.org/wiki/Band_gap

[40] G. L. Tan, M. F. Lemon, D. J. Jones and R. H. French. "Optical properties and London dispersion interaction of amorphous and crystalline SiO_2 determined by vacuum ultraviolet spectroscopy and spectroscopic ellipsometry". Phy. Rev. B, vol. 72, no. 20, pp. 205117-1 - 205117-10, 2005. https://doi.org/10.1103/PhysRevB.72.205117.

[41] Q. Wang, J. Wen, Y. Luo, G-D Peng, F. Pang, Z. Chen, and T. Wang. "Enhancement of lifetime in Er-doped silica optical fibre by doping Yb," *Opt. Mat. Exp.,* vol. 10, no. 2, pp. 397–407, 2020. https://doi.org/10.1364/OME.381237.

[42] Y. Yue, Y. Song, and X. Zuo, "First principles study of oxygen vacancy defects in amorphous SiO_2," AIP

Advances, vol. 7, no. 1, p. 015309, 2017. http://dx.doi.org/10.1063/1.4975147.

[43] H. M. Lawler, J. J. Rehr, F. Vila, S. D. Dalosto, E. L. Shirley and Z. H. Levine. "Optical to UV spectra and birefringence of SiO_2 and TiO_2: First-principles calculations with excitonic effects". Phy. Rev. B, vol. 78, no. 20, pp. 205108-1 – 205108-8, 2008. https://doi.org/10.1103/PhysRevB.78.205108.

[44] S. Abedrabbo, B. Lahlouh, A. T. Fiory and N. M. Ravindra. "Optical polarizability of erbium-oxygen complexes in sol-gel-based silica films". J. Phy. D: App. Phy., vol. 54, no. 13, pp. 135101, 2021. DOI 10.1088/1361-6463/abd5e4.

[45] A. J. Chekol, S. M. Sipaut, and V. Padavettan. "Size-dependent physicochemical and optical properties of silica nanoparticles". *Colloid J.,* vol. 10, pp. 201–209, 2009.

[46] Z. A. Wahab et al. "Characterization and optical properties of erbium oxide-doped ZnO–SLS glass". *Mat. Exp.,* vol. 7, pp. 60–68, 2017. DOI: 10.1166/mex.2017.1388.

[47] S. A. Kamil. "Local structural analysis of erbium-doped tellurite modified silica films". *Mat. Res. Exp., vol.* 5, pp. 105009, 2018. DOI: 10.1088/2053-1591/aad4ad.

[48] J. Li et al. "Overview of radiation induced point defects in silica-based optical preforms". *Opt. Mat. Exp., vol.* 9, pp. 1130–1157, 2019. DOI: 10.1364/OME.9.001130.

[49] A. M. Mansour, A. B. Abou Hammad and A. M. El Nahrawy. "Synthesis and Optical Properties of Erbium-Doped Sodium Silicate in Sol-Gel Matrix". Si, vol. 16, pp. 3719–3727, 2024.

[50] C. M. Carbonaro, V. Fiorentini and S. Massidda. "Ab-initio study of oxygen vacancies in alpha-quartz". J. of Non-Cryst. Solids, vol. 221, no. 1, pp. 89-96, 1997. https://doi.org/10.1016/S0022-3093(97)00286-X.

[51] A. Polman, D. C. Jacobson, D. J. Eaglesham, R. C. Kistler and J. M. Poate. "Optical doping of waveguide materials by MeV Er implantation". J. App. Phy. vol. 70, pp. 3778–3784, 1991.

[52] J. L. Bischoff and D. Vanderbilt. "First-principles calculations of the E' centre in amorphous SiO_2". *Phy. Rev. B*, vol. 61, no. 12, pp. 8183–8190, 2000. https://doi.org/10.1103/PhysRevB.61.8183

[53] J. R. Tumsa and S. T. Mukhopadhyay. "The role of oxygen vacancies in water splitting photoanodes". Energy Env. Sci., vol. 13, pp. 1312–1330, 2020.

[54] G.M. Lo Piccolo, M. Cannas, and S. Agnello, "Intrinsic point defects in silica for fibre optics applications", Materials, 14(24), P 7682, 2021. https://doi.org/10.3390/ma14247682.

[55] C. M. Herzinger, B. Johs, W. A. McGahan, J. A. Woollam and W. Paulson. "Ellipsometric determination of optical constants for silicon and thermally grown silicon dioxide via a multi-sample, multi-wavelength, multi-angle investigation". J. App. Phy., vol. 83, pp. 3323–3336, 1998.

[56] M. N. Polyanskiy. "Refractive index.info database of optical constants," Sci. Data, vo. 11, pp. 94, 2024.

[57] J. M. Wagner. "Ab initio calculation of optical absorption and reflectivity of $Si(001)/SiO_2$ superlattices with varying interfaces". App. Surf. Sci., vol. 255, pp. 6421–6427, 2009.